

Static dielectric properties of carbon nanotubes from first principles

Boris Kozinsky¹ and Nicola Marzari²¹Department of Physics, MIT, Cambridge, MA 02139²Department of Materials Science and Engineering, MIT, Cambridge, MA 02139

(Dated: April 14, 2024)

We characterize the response of isolated single- (SW NT) and multi-wall (MW NT) carbon nanotubes and bundles to static electric fields using first-principles calculations and density-functional theory. The longitudinal polarizability of SW NTs scales as the inverse square of the band gap, while in MW NTs and bundles it is given by the sum of the polarizabilities of the constituent tubes. The transverse polarizability of SW NTs is insensitive to band gaps and chiralities and is proportional to the square of the effective radius; in MW NTs the outer layers dominate the response. The transverse response is intermediate between metallic and insulating, and a simple electrostatic model based on a scale-invariance relation captures accurately the first-principles results. Dielectric response of non-chiral SW NTs in both directions remains linear up to very high values of applied field.

PACS numbers: 73.63.Fg; 77.22.Ej; 85.35.Kt

Carbon nanotubes attract a lot of scientific interest due to their unique and versatile electronic and mechanical properties, suitable for a wide range of applications. Nanotubes have different electronic properties, determined in the zone-folding scheme by the chiral vector: arm chair (m, m) nanotubes are 1D metals, and zigzag $(m, 0)$ nanotubes are semiconductors, with (almost) vanishing gaps for $m = 3n$. Synthesis and separation of specific nanotubes remains a central challenge. Variations in chirality and size influence dielectric properties, which in turn can be exploited for separation; e.g. electric fields have been used to align nanotubes during PECVD synthesis [1, 2] and to separate different tubes in solutions [3]. A detailed physical understanding of dielectric response is also needed to characterize optical excitations, screening at contacts, plasmons in nanotube arrays, and the degree of control achievable on endohedral fillings. While in recent years the response of SW NTs has been studied with tight-binding [4, 5, 6] and first-principles approaches [7, 8], MW NTs (a more common product of synthesis) have received much less attention due to their complexity. We present here a comprehensive and detailed picture of dielectric screening in SW NTs, MW NTs and bundles, using a combination of first-principles techniques and introducing an accurate classical electrostatic model that captures the unusual response of these materials.

All calculations are performed using Quantum-ESPRESSO [9] with the PBE approximation and ultrasoft pseudo-potentials in a plane-wave basis. A tetragonal unit cell is set up with periodic-boundary conditions in all three dimensions. A k -point sampling grid of at least $30 \times 1 \times 1$ points is used; this is sufficient to converge polarizabilities to within 3 significant digits. Atomic configurations are generated using an interatomic distance of 1.42 \AA , obtained from careful relaxation studies [10]. Longitudinal and transverse polarizabilities are calculated using density-functional perturbation theory (DFPT) [11] and finite-field or electric-enthalpy approaches [12],

also implemented in our Quantum-ESPRESSO code. Since we use periodic-boundary conditions, we effectively simulate a three-dimensional bulk material consisting of a square array of infinite parallel nanotubes. The longitudinal dielectric response of an isolated nanotube is characterized by polarizability per unit length κ , which is related to the separation-dependent bulk dielectric constant ϵ_k using the relation

$$\epsilon_k = 1 + \frac{4}{\kappa} \quad (1)$$

where $\Omega = L^2$ is the cross-sectional area of the unit cell. From linear-response theory [13] we expect the static dielectric constant to depend on the gap as $\epsilon(q) \sim 1 + (\hbar v_F / E_g)^2$ which suggests via (1) that $\kappa \sim 1/E_g^2$. Our calculations confirm this behavior in zigzag nanotubes, as shown in Fig. 1. As expected, $(9,0)$, $(12,0)$ and $(15,0)$ nanotubes have the smallest gaps and the largest κ ; the inverse-square dependence on the gap roughly holds over two orders of magnitude. Only the narrowest nanotubes $(7,0)$ and $(8,0)$ deviate from this trend. The agreement is particularly accurate for large-gap zigzag nanotubes $(3n+1,0)$ and $(3n+2,0)$ with $n > 2$. We note in passing that for these SW NTs our first-principles results can be fitted well with these relations: $E_g \approx 3.3 R_0 + 0.06$ and $\kappa \approx 8.2 R_0^2 + 20.5$, with E_g in eV and R_0 in Å. Previous tight-binding studies [4] reported values of κ comparable to ours, and noted a relation $\kappa \sim R_0^2/E_g^2$ which we also observe for large-gap nanotubes (see Fig. 1). For infinitely-long arm chair SW NTs the longitudinal polarizability per unit length κ diverges since there is no gap in the band dispersions. To get a sense of scaling we can approximate such nanotubes as metallic ellipsoids of length l and transverse radius R ($l \gg R$); the classical result is $\kappa \approx \frac{2}{3} 4\pi \epsilon_0 (l/R) \approx 24 (\ln(l/R) - 1)$. For MW NTs, the longitudinal picture remains simple: depolarization effects along the axis are negligible, and constituent tubes have very weak dielectric interactions. The total polarizability

TABLE I: Radius, band gap, longitudinal and transverse polarizabilities (per unit length) of carbon nanotubes as a function of the chiral vector $(n;m)$.

$(n;m)$	R_0 (Å) ^a	g (eV)	α_{\parallel} (Å ²)	α_{\perp} (Å ²)
(7,0)	2.74	0.48	6.47	83.0
(8,0)	3.15	0.57	7.80	104
(9,0)	3.58	0.17	9.32	1460
(10,0)	3.95	0.91	10.9	142
(11,0)	4.34	0.77	12.7	186
(12,0)	4.73	0.087	14.3	6140
(13,0)	5.09	0.72	16.3	224
(14,0)	5.48	0.63	18.4	279
(15,0)	5.88	0.041	20.3	11100
(16,0)	6.27	0.61	22.9	326
(17,0)	6.66	0.53	25.2	395
(8,0)+(17,0)	–	–	25.8	499
(8,0)+(16,0)	–	–	23.6	427
<hr/>				
(4,4)	2.71	(0)	6.41	(1)
(5,5)	3.40	–	8.71	–
(6,6)	4.10	–	11.6	–
(7,7)	4.76	–	14.7	–
(8,8)	5.45	–	18.1	–
(9,9)	6.12	–	21.8	–
(10,10)	6.78	–	26.1	–
(12,12)	8.14	–	35.8	–
(14,14)	9.50	–	47.2	–

^a R_0 is the radius of the carbon backbone

$\alpha_{\parallel}^{\text{tot}}$ should then simply be the sum of the polarizabilities of constituent SW NTs; this conclusion is confirmed by our results in Table I.

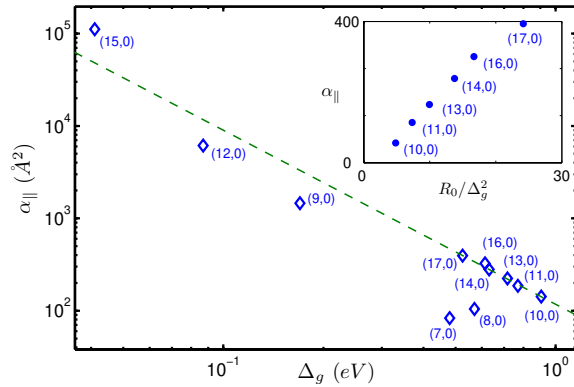


FIG. 1: Log scale plot of α_{\parallel} of zigzag nanotubes as a function of band gap. The dashed line has slope -2. The inset shows the values for large-gap SW NTs as a function of $R_0 = \frac{2}{g}$.

We address the characterization of the transverse dielectric response in two different ways. First, we calculate with DFPT the dielectric constant ϵ_{\perp} , from which

TABLE II: Transverse polarizabilities of MW NTs.

MW NT	α_{\perp} (Å ²) (ab-initio)	α_{\perp} (Å ²) (model)
(8,0)+(17,0)	25.8	25.7
(5,5)+(10,10)	26.8	26.6
(4,4)+(12,12)	36.1	36.0
(9,9)+(14,14)	49.0	48.2
(4,4)+(9,9)+(14,14)	49.1	48.3

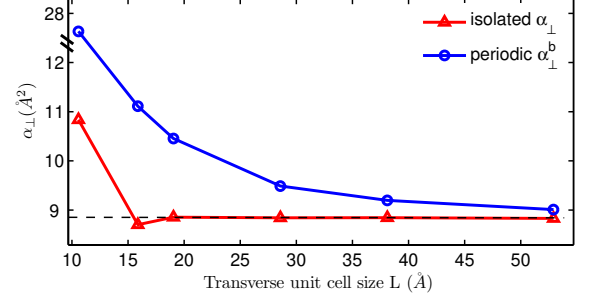


FIG. 2: Convergence of α_{\perp} and α_{\perp}^b with respect to L for a (5,5) SW NT. The point at $L = 10.6$ Å corresponds to a typical tube-tube separation in a bundle.

the transverse polarizability α_{\perp} is extracted. To study non-linear dielectric effects, we also obtain α_{\perp}^b by applying an electric field E_{out} via a sawtooth potential, and computing the total induced dipole moment per unit length p_{\perp} . In the linear regime the two approaches are equivalent, and we find an agreement between the two methods within 1%. Both DFT-based calculations take into account the local-field effects, that would be absent in tight-binding calculations. Again, since calculations provide us with the transverse response of a periodically-repeated array of nanotubes, it is necessary to remove the depolarization fields stemming from the periodic images. In principle one could use

$$\alpha_{\perp}^b = \frac{p_{\perp}}{4} (\epsilon_{\perp} - 1) = \frac{p_{\perp}}{E_{\text{out}}} \quad (2)$$

for the first and second methods respectively, while taking the limit $L \rightarrow \infty$ for which the depolarization fields vanish. In practice, these persist for very large inter-tube separations due to the long range of electrostatic interactions between image tubes. Computation time grows as L^2 at a fixed energy cutoff, quickly becoming unmanageable without even reaching a converged result; Fig. 2 illustrates the slowness of this convergence. It is clear, however, that at large separations only electrostatic effects are important, so we can solve this problem using a classical 2D Clausius-Mossotti correction [14] relating the single-tube polarizability α_{\perp} to the periodic bulk L -dependent value α_{\perp}^b . The relevant conversions are

$$\epsilon_{\perp} = \frac{\alpha_{\perp}}{2} \frac{1}{\alpha_{\perp} + 1} = \frac{\alpha_{\perp}^b}{1 + \frac{2}{\alpha_{\perp}^b}} \quad (3)$$

The values of α_\perp obtained from (3) are listed in Table I and plotted in Fig. 3 as a function of the square of the effective outer radius $\tilde{R} = R_0 + 1.3A$ (see later discussion). Remarkably, transverse polarizabilities of both metallic and semiconducting SWNTs lie on the same curve, which can be fitted by a line $\alpha_\perp = c\tilde{R}^2$ with slope $c = 0.40$. Thus chirality and longitudinal band structure have a negligible effect on the transverse dielectric response; this was observed in earlier calculations [4, 7, 8] and justified with symmetry arguments in the single-particle approximation [4]. Recent tight-binding calculations [5, 6] predict a small and systematic difference between polarizabilities of metallic and semiconducting SWNTs; however, we do not detect these differences in our DFT calculations.

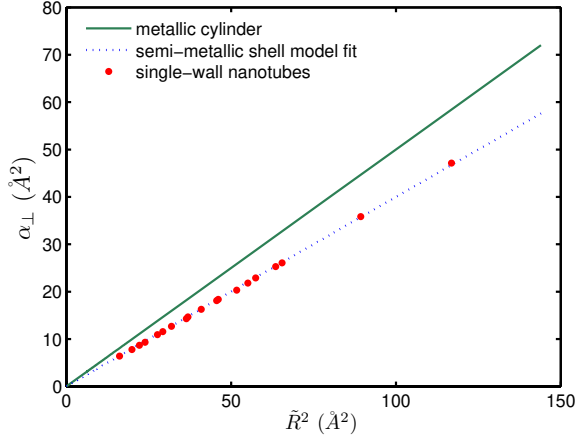


FIG. 3: Transverse polarizabilities α_\perp of arm chair and zigzag nanotubes as a function of \tilde{R}^2 . The dashed line is the best-fit result of our semi-metallic shell model; the solid line $\alpha_\perp = \frac{1}{2}\tilde{R}^2$ corresponds to an ideal metallic cylinder.

Periodic boundary conditions allow us to easily examine the bulk dielectric response of nanotube bundles. We compute ϵ_\perp and ϵ_\parallel of triangular and square arrays with inter-tube separation of $d = 3.4A$ [15]. The values of ϵ_\parallel accurately match those computed from ϵ_\parallel of isolated nanotubes using (1), thus reflecting the additive property of the longitudinal response. In contrast, transverse response of bundles depends strongly on d . Fig. 2 illustrates both the benefits of using the Clausius-Mossotti relation (3) for large d , and the limitation of its applicability when d is small. Whereas the longitudinal response remains simple, the transverse dielectric tensor at small d may have sizeable anisotropic and off-diagonal contributions depending on the combined point-group symmetry of the nanotube and the lattice. These contributions vanish quickly with d and do not affect our isolated tube calculations.

By applying a finite transverse field E_{out} we can also study screening inside a nanotube; we find the inner field E_{in} to be very uniform, as shown in Fig. 4. An-

other remarkable feature is that the screening factor $E_{\text{out}} = E_{\text{in}} = 4/3 \approx 0.1$ turns out to be independent of radius and chirality for all SWNTs. To make physical sense of these general results we look for a simple electrostatic model that would capture these traits. A solid dielectric cylinder of radius \tilde{R} and bulk dielectric constant would have polarizability $\alpha_\perp = \frac{1}{2} \frac{\epsilon - 1}{\epsilon + 1} \tilde{R}^2$, a uniform inner field and a screening factor $E_{\text{out}} = E_{\text{in}} = (\epsilon + 1)/2$ independent of radius. This picture, however, does not correspond to a nanotube, where screening is accomplished by a thin layer of delocalized π -electrons. One could then treat a nanotube as a dielectric cylindrical shell of finite thickness. In this case the inner field remains uniform, but the screening factor decreases with increasing radius. To identify an appropriate model that incorporates all the observed features, we note that in general a radius-independent uniform inner field is produced by the surface charge density $\sigma(\theta) = \sigma_0 \cos(\theta)$, where θ is the angle measured from the direction of E_{out} . The dipole moment per unit length in this case is $p_\perp = \sigma_0 \tilde{R}^2 = \alpha_\perp E_{\text{out}}$ and the polarizability is $\alpha_\perp = \frac{p_\perp}{E_{\text{out}}} \tilde{R}^2 = c \tilde{R}^2$ with $c = 1/2$. In a metallic cylinder c is $1/2$ and the outer field is completely screened. A best fit of our ab-initio data for SWNTs to this model (see Fig. 3) yields the slope $c = 0.40$ and effective radius $\tilde{R} = R_0 + 1.3A$ larger than the radius of the carbon backbone R_0 , consistent with the finite thickness of the electronic charge density distribution. Elementary electrostatic considerations yield a screening factor $E_{\text{out}} = E_{\text{in}} = \frac{1}{1 - 2c} = 5$ in good agreement with our finite-field calculations and previous estimates [4, 5]. It should be stressed that the screening properties of nanotubes, reflected in this model, are neither metallic nor insulating. This peculiarity is physically grounded in the fact that in a single sheet of graphite the screening of Coulomb interactions is anomalous due to the vanishing density of states at the Fermi points [16]. For carbon nanotubes (as opposed to boron-nitride nanotubes), the semi-metallic nature of π -electrons implies that the screening factor is radius-invariant.

The generalization of this model to the multi-wall case needs to take into account screening and electrostatic interactions between layers. Our strategy is to first solve exactly the general problem of N concentric dielectric cylindrical shells in a uniform field. We then recover precisely the above single-layer model by treating a SWNT as a shell of radius \tilde{R} , dielectric constant ϵ and vanishing thickness δ , and constraining these parameters by the scale-invariance condition

$$\frac{\epsilon - 1}{\tilde{R}} = \frac{4c}{1 - 2c} = \text{const} \quad (4)$$

that guarantees that the screening factor remains independent of \tilde{R} . Modelling a general MWNNT amounts to solving a linear system of $2N - 2N$ boundary-condition equations [17] containing the best-fit parameters c and \tilde{R} (carried over from the single-wall case) and subject

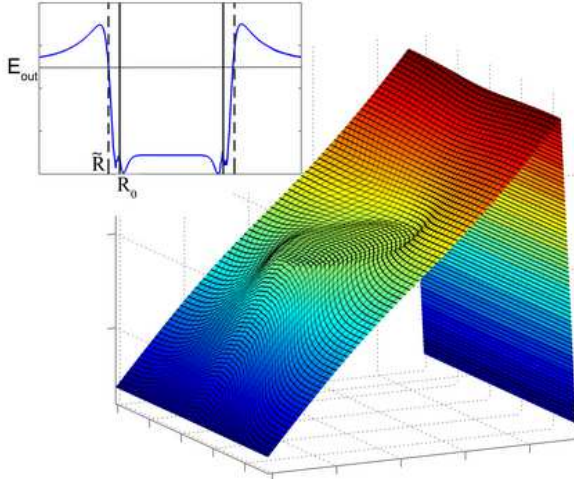


FIG. 4: Electrostatic potential for a (10,10) SW NT in an applied homogeneous transverse field E_{out} . The electric field through the center slice is shown in the inset.

to constraint (4). For the double- and triple-wall cases we find excellent agreement between this model and our ab-initio results (see Table II). We conclude that the present semi-metallic shell model captures all characteristics of the transverse dielectric response: uniform inner field, radius-independent screening factor in SW NTs, and correct ϵ_{\perp} for MW NTs. We note also that the largest contributions to transverse polarizabilities come from the outer few layers, and inner layers play a negligible role due to a combination of screening and their smaller radii. Diameter control alone thus becomes the key growth-parameter determining transverse response.

The finite-field approach is also used to determine the range of fields for which the transverse dielectric response is linear. The (5,5) nanotube exhibits precisely linear response with the same polarizability coefficient to within 3 significant digits for field magnitudes of 0.05, 0.5, 5 V/nm, the last one being greater than the experimentally attainable value. This implies that our electrostatic shell model of transverse response remains valid in the regime of large applied fields. To study the linearity of longitudinal response, we minimize directly the electric-enthalpy functional [12] to introduce a finite longitudinal field while preserving periodic-boundary conditions. We find that the longitudinal response of the (8,0) nanotube becomes nonlinear by only 5% at $E_k = 0.5$ V/nm. Nonlinearity is in fact suppressed because zigzag and arm chair (non-chiral) nanotubes are center-symmetric, so the first hyper-polarizability vanishes by symmetry [7]. To estimate the second hyper-polarizability χ_k we compute polarizations at several values of the field, and fit the result to the expression $P = \epsilon_k E + \chi_k E^3$. We obtain $\epsilon_k = 106$ Å² (in agreement with the DFPT result in Table I) and $\chi_k = 3.1 \times 10^7$ in atomic units.

We now turn to the question of alignment of nanotubes

in a uniform electric field. The torque on a nanotube of length l at an angle θ to the field E is

$$\tau = \frac{1}{2} \frac{d}{d\theta} (E^2 \sin^2 \theta) = E^2 \sin \theta \cos \theta \quad (5)$$

The longitudinal and transverse polarizabilities compete with each other, but our results imply that $\epsilon_k > \epsilon_{\perp}$ in all nanotubes, much more so in metallic and small-gap semiconducting nanotubes. Indeed, for all nanotubes $\epsilon_{\perp} < \frac{1}{2} R_0^2$ whereas for large-gap SW NTs $\epsilon_k > 8.2 R_0^2$, and for MW NTs ϵ_k is additive while ϵ_{\perp} is not. So nanotubes of all types will align with the electric field, but by tuning the value of the field during PECVD growth it may be possible to selectively grow highly polarizable (e.g. metallic) tubes.

There have also been attempts to separate semiconducting and metallic nanotubes in solution using inhomogeneous electric fields [3]. A polarized nanotube aligned with the field will be pulled in the direction of or against the field gradient, depending on its effective dielectric constant ϵ_k relative to that of the solvent ϵ_s . Assuming no solvent inside the nanotube, and approximating it by a solid dielectric cylinder of radius R_0 , we obtain from our values of ϵ_k an effective $\epsilon_k = 1 + 4 \epsilon_k R_0^2 / 30$ for large-gap semiconducting SW NTs and obviously much larger values for small-gap and metallic tubes. This result is consistent with findings that only metallic SW NTs are observed deposited on the electrodes in water ($\epsilon_s = 80$), whereas all nanotubes are drawn towards the electrodes in isopropylalcohol ($\epsilon_s = 18$).

In summary, we studied in detail the dielectric properties of isolated and bundled SW NTs and MW NTs. In SW NTs, the longitudinal response is controlled by the band gap, while the transverse response is sensitive only to the effective radius. In bundles and MW NTs longitudinal response is additive, while the transverse response in MW NTs is dominated by the outer few layers. We presented an accurate scale-invariant electrostatic model of transverse response, which is intermediate between that of a metal and an insulator. The authors would like to thank L. S. Levitov for valuable suggestions. This work was supported by NSF-NIRT DMR-0304019 and the Singapore-MIT alliance.

-
- [1] Y. Zhang et al, Appl. Phys. Lett. 79, 3155 (2001); A. Ural et al, Appl. Phys. Lett. 81, 3464.
 - [2] J. Yu et al, J. Vac. Sci. Technol. B, 19, 671 (2001).
 - [3] R. K. Nipke et al, Science 301, 344 (2003); J. Li et al, Appl. Phys. Lett. 86, 153116 (2005).
 - [4] L. X. Benedict, S. G. Louie and M. L. Cohen, Phys. Rev. B 52, 8541 (1995).
 - [5] D. S. Novikov and L. S. Levitov, cond-mat/0204499.
 - [6] Y. Li, S. V. Rotkin, U. Ravaioli, Nano Lett. 3, 183 (2003).
 - [7] G. Y. Guo et al, Phys. Rev. B 69 205416 (2004).
 - [8] E. N. Brothers et al, Phys. Rev. B 72, 033402 (2005).

- [9] S. Baroni et al, <http://www.quantum-espresso.org>.
- [10] N. Mounet, M. Sc., MIT (2005); N. Mounet and N. Marzari, Phys. Rev. B 71, 205214 (2005).
- [11] S. Baroni et al, Rev. Mod. Phys. 73, 515 (2001).
- [12] I. Souza, J. Iniguez and D. Vanderbilt, Phys. Rev. Lett. 89, 117602 (2002); P. Umari and A. Pasquarello, *ibid.* 89, 157602 (2002).
- [13] D. R. Penn, Phys. Rev. 128, 2093 (1962).
- [14] F. J. Garcia-Vidal, J. M. Pitarke and J. B. Pendry, Phys. Rev. Lett. 78, 4289 (1997); L. Wirtz et al, Phys. Rev. B 71, 241402(R) (2005); J. Tobik and A. Dal Corso, J. Chem. Phys. 120, 9934 (2004).
- [15] S. Agnietti et al, Langmuir 21, 896 (2005); M. F. Lin, Phys. Rev. B 62, 13153 (2000).
- [16] J. Gonzalez et al, Nucl. Phys. B 424, 595 (1994); *ibid.*, Phys. Rev. B 63, 134421 (2001).
- [17] Matlab script: <http://quasiamore.mit.edu/CNT/dielec.html>